



<https://doi.org/10.21203/rs.3.rs-1543477/v1>

This work is licensed under a Creative Commons Attribution 4.0 International License. [Read Full License](#)



1  
2  
3  
4 Improved Complete Ensemble Empirical Mode  
5

6 Decompositions with Adaptive Noise of Global, Hemispherical  
7 and Tropical Temperature Anomalies, 1850-2021  
8  
9

10 Charles D. Coleman

11 ORCID: <https://orcid.org/0000-0001-6940-8117>  
12  
13  
14

15 Received: date / Accepted: date  
16  
17

18 Abstract ICEEMDAN, a variant of Empirical Mode Decomposition (EMD), is used to extract  
19 temperature cycles with periods from half a year to multiple decades from the HadCRUT5  
20 global temperature anomaly data. The residual indicates an overall warming trend. The analysis  
21 is repeated for the Southern and Northern Hemispheres as well as the Tropics, defined  
22 as areas lying at or below 30 degrees of latitude. Multiannual cycles explain the apparently  
23 anomalous pause in global warming starting around 2000. The previously identified multi-  
24 decadal cycle is found to be the most energetic and to account for recent global warming  
25 acceleration, beginning around 1993. This cycle's amplitude is found to be more variable  
26 than by previous work. Moreover, this variability varies by latitude. Sea ice loss accelera-  
27 tion is proposed as an explanation for global warming acceleration.

28 Keywords global warming · climate cycles · global warming acceleration · time series  
29 analysis · climate change · Hilbert-Huang transform  
30

31  
32  
33 1 Introduction  
34

35 Long-term variation in global temperatures is a well-known phenomenon. Improved Complete  
36 Ensemble Empirical Mode Decomposition with Adaptive Noise (ICEEMDAN, Colom-  
37 inas Schlotthauer and Torres 2014), a variant of the Empirical Mode Decomposition (EMD,  
38 Huang, Shen et al. 1998) decomposes time series of temperature anomalies into Intrinsic  
39 Mode Functions (IMFs) representing noise, cycles of different and possibly nonconstant fre-  
40 quencies and amplitudes and a residual. The last estimates the trend in temperature  
41 anomalies. Colominas, Schlotthauer and Torres 2014 developed ICEEMDAN as an  
42 improvement

43 This article represents personal work by the author. Therefore, the U.S. Census Bureau can bear no responsi-  
44 bility for its contents.

55  
56  
57  
58  
59  
60  
61  
62  
63  
64  
65

45 C.D. Coleman  
46 U.S. Census Bureau *Present address:* C.D. Coleman  
47 5811Alexandria, VA 22310Governors View Ln.  
48 USA  
49 E-mail: chuckcoleman@yahoo.com  
50  
51  
52  
53  
54

1 on prior EMD variants to more accurately reproduce the input signal and to reduce the re-  
2 maining residual noise. They show that ICEEMDAN extracts signals more faithfully and

3  
4 with less residual noise than Ensemble Empirical Mode Decomposition (EEMD) (Wu and<sup>1</sup>  
5 Huang 2009).

6 The temperature anomaly data come from the Met Office Hadley Centre HadCRUT5  
7 infilled observation datasets. (Dunn and Hogan in press) The data are for months between  
8 January, 1850 and December, 2019. For each 5° by 5° cell of the Earth's surface, the aver-  
9 age temperature, 1961-1990, is computed. A monthly time series of temperature  
anomalies

10 is constructed for each cell by subtracting the 1961-1990 average from the monthly esti-  
11 mated values. The averaged series are the averages of the anomalies for the area of  
interest,

12 weighted by surface area. All available averaged series are used: global and Northern and  
13 Southern Hemispheres. In addition, a tabulation was obtained from the Met Office  
Hadley 14 Centre for the Tropics, defined as latitudes between 30°N and 30°S. The mean  
for each 15 series is used as the measure of temperature.

## 16 17 18 2 Previous Research 19

20 Previous research has followed four approaches. The first has concentrated on removing  
21 noise by smoothing data. The popularly displayed annual averages of Lindsey and Dahlman  
22 (2020) and others are simply the average of all months within a calendar year. Not only is  
23 the choice of periods to smooth is arbitrary, the smoothed data prevent identification  
of bien-

24 nial, annual and subannual cycles. Moreover, identification of multiannual data is hampered  
25 by preventing the contributions of individual months from being identified. Variations in the  
26 timing of cycles with periods of a few years can result in their nonidentification. Hansen  
et

27 al. (2006) avoided this by focusing on the changes over time and not attempting any decom-  
28 positions or forecasts. Hansen, Sato and Ruedy (2013) similarly use annual averages in an  
29 analysis of climatic forcing. Hansen and Sato (2021) use a linear trend to identify putative 30  
recent global warming acceleration. A 21-year weighted moving average has happily been  
31 discontinued from the Internet.

32 The second approach is regression analysis. Foster and Rahmstorf (2011) and Zhou and  
33 Tung (2013) use linear regression on global data to obtain linear trends after controlling  
34 for forcing variables. The obvious criticisms are that the trends are not necessarily linear,  
35 the forcing variables may not have linear effects, missing variables may be present and  
that 36 the time series structure is not used in any way. Lean and Rind (2008) partition  
the Earth's

37 surface into cells, then run regressions within each cell and combine results. This approach  
38 suffers from not explicitly incorporating the spatial structure in what is really a spatial panel  
39 model. An additional weakness of regression is that statistical significance does not imply  
40 practical significance (Ziliak and McCloskey 2004; McCloskey and Ziliak 2008). When a  
41 variable lacks practical significance, controlling for it has no practical effect on regression  
42 fit. Turner, Colwell et al. (2005) use regression analysis on monthly Antarctic temperature  
43 and wind speed data to obtain linear trends. This approach has the defects of assuming 44  
linearity and not accounting for time series structure. Thus, their results suffer from bias 45  
and, at best, can only be interpreted qualitatively.

46 The third approach uses wavelet analysis. A full description of wavelet analysis is be-  
47 yond the scope of the present paper. A short description is that a basis function is chosen  
48

---

49 <sup>1</sup>Torres, Colominas and Schlotthauer 2014, Figure 2, does not display ICEEMDAN's two residual IMFs  
50 for that example while displaying all five of EEMD's residual IMFs.  
51  
52  
53  
54  
55  
56  
57  
58  
59  
60  
61  
62  
63  
64  
65

that, in turn, generates other basis functions that are used to form a wavelet  
representation of a signal. The exact representation depends on the choice of initial basis function.  
Recovering amplitude and frequency information is mathematically complicated. Lau and Weng (1999),  
Silva, Silva et al. (2018) and Yang, Wang et al. (2015) are examples of applying wavelet analysis to monthly  
temperature data. The starting dates of these analyses, 1884 (Silva, Silva et al. 2018) and 1955 (Lau and  
Weng 1999; Yang, Wang et al. 2015), show an important limitation: these analyses do not use the full  
time series because of the initial noise, as described in Section 4. Moreover, the trends are linear, a  
constraint that EMD lacks. 10 Empirical Orthogonal Functions (EOFs) appear to have fallen out of favor  
in climatic 11 research. EOFs are the principal components of spatiotemporal data (Bjornsson and  
Venegas" 12 2000). The components are called "modes of variability," Their problem lies in their being  
13 "primarily *data modes, and not necessarily physical modes*" (Bjornsson and Venegas 2000,"

14 p. 5, original emphasis). Without physical knowledge, they provide little information about  
15 physical phenomena. Examples of their application to climatic data, including global  
warm16 ing, include Bjornsson and Venegas (2000), Bretherton, Widman et al. (1999),  
Feldstein" 17 (2002) and Wang and Mehta (2008).

55  
56  
57  
58  
59  
60  
61  
62  
63  
64  
65

18 The last approach uses the data-driven Empirical Mode Decomposition (EMD) or Ensemble  
 Empirical Mode Decomposition (EEMD) (Wu and Huang 2009) and seems to be the  
 20 most popular recently. Section 3 delves into the technical details. Huang, Wu et al. (2009)  
 21 appear to have been the first. They use EMD to remove noise from monthly global temper-  
 22 ature anomaly series to derive annual series. Wu, Huang et al. (2011) essentially repeat the  
 23 analysis using EEMD and identify a nearly regular multidecadal cycle. Franzke (2010) uses  
 24 EEMD to remove noise from Antarctic temperature series to identify trends. Shi, Yang et  
 25 al. (2011) and Xing, Chen et al. (2016) apply EEMD to tree ring records. Qian (2015) uses  
 26 EEMD to remove noise from Shanghai, China temperature extreme series to identify the  
 27 effects of urbanization on them. Yang, Wu and Hu (2011) apply EMD to air temperature ob-  
 servations at Nanjing, China to find no detectable solar-driven variability, which the  
 present paper confirms globally. Mukherjee, Joshi et al. (2014) apply EEMD to daily  
 Indian monsoon rain totals. Similarly, Sabzehee, Nafisi et al. (2019) analyze Caspian Sea  
 catchment  
 31 rain totals.

### 34 3 Empirical Mode Decomposition

35  
 36 Huang, Shen et al. (1998) introduced the Empirical Mode Decomposition (EMD) as an adap-  
 tive,  
 data-driven method to completely decompose time series using the Hilbert Transform.  
 38 The Hilbert Transform is a more general version of the Fourier Transform, decomposing a  
 39 time  
 series into the sum of series of the form

$$40 \quad \phi_j(t) = a_j(t) \sin(\omega_j(t)t + \theta_j(t)) \quad (1)$$

41  
 42 where  $a_j$  is the amplitude of  $\phi_j$ ,  $\omega_j$  is its possibly time-varying period and  $\theta_j$  is its possibly  
 43 time-varying phase shift. The true  $\phi_j$  are the modes of the input signal. The estimates  $\hat{\phi}_j$   
 44 are Intrinsic Mode Functions (IMFs) which should satisfy the condition that the number  
 of  
 45 extrema should differ from the number of zero-crossings by 0 or 1. Given a residue  
 $r_j$ , with

46  $r_0$ , the initial residue equal to the input signal, EMD proceeds to sift  $r_j$  to produce  $\text{IMF}^{j+1}$   
 47 and  $r_{j+1}$  by first constructing upper and lower envelopes by interpolating the local maxima  
 48 and minima, respectively, then subtracting their local means from  $r_j$  to obtain  $h_j$ . If  $h_j$  is  
 an  
 49 IMF, then it is output as  $\text{IMF}^{j+1}$  and  $r_{j+1}$  is set equal to  $r_j - h_j$ . Otherwise, the algorithm  
 50 repeats, using  $r_{j+1}$  and iterated until an IMF is produced or a stopping criterion is  
 reached, 51

52  
 53  
 54  
 1 in which case a defective IMF is output. IMFs are subsequently output until  $r_j$  has 2 or 3  
 2 extrema, in which case it is output as the residual trend. EMD ideally outputs IMFs in order  
 3  
 4 of increasing period or, equivalently, decreasing frequency.

5 EMD is well-known for mode-mixing (outputting a single IMF for multiple  $\phi_j$ ), mode  
 6  
 splitting (outputting multiple IMFs for a single  $\phi_j$ ) and producing spurious IMFs. Several  
 7  
 methods have been developed to remedy this, including EEMD, CEEMDAN (Schlotthauer,  
 8  
 Colominas et al. 2011), ICEEMDAN and MAEMD (Deering and Kaiser 2005). These meth-  
 9  
 ods are all ensemble methods that add a function to multiple copies of the input, then  
 average

10 the outputs. This enables them to reduce EMD's mode-mixing and mode-splitting (Huang,  
 11 Shen et al. 1998). The first two add white noise, ICEEMDAN adds IMFs derived from white  
 12 noise and MAEMD adds and subtracts a masking sinusoid. All average the results of their  
 13 decompositions. Ensemble methods have the further advantage of being able to separate the  
 14 noise which EMD lacks (Kim, Kim and Oh 2012). Ensemble methods are not guaranteed to  
 15 produce proper IMFs because the average of IMFs is not necessarily an IMF (Steven San1 6  
 doval personal communication). All EMD methods are subject to outputting residual IMFs  
 17 due to possible nonorthogonality of the IMFs that represent the input signal The summed  
 18 IMFs are subtracted from the temperature anomaly input to obtain the temperature trend,  
 19 with the obvious interpretation. Colominas et al. (2014) showed that ICEEMDAN outputs  
 20 IMFs in decreasing order of frequency with fewer residual IMFs than EMD, EEMD and  
 21 CEEMDAN and does not output residual IMFs before outputting all informative IMFs.  
 22 ICEEMDAN is run with 10,000 ensemble members and the default SNR of 0.2. The  
 num23 ber of ensemble members was empirically determined to provide stable  
 decompositions. 24 The number of IMFs was set to 8 to avoid residual IMFs and to include  
 a residual ninth IMF 25 in the residual trend.

26 EMD has the further advantage of being applicable to any type of time series. Fourier  
 27 series have the tightest restrictions: linearity and stationarity. Wavelets permit  
 nonstation28 arity but require linearity. Fourier series and wavelets require a priori  
 bases, while EMD is 29 adaptive. EMD is chosen to minimize assumptions.

#### 32 4 Results

34 This Section presents selected graphs illustrating the temperature anomaly  
 decompositions  
 35 and provides some interpretations . The decompositions were performed for all  
 downloaded  
 36 series. R (2020) codes, an R workspace and undisplayed graphs are in the Supplemental  
 37 materials. Additionally, for each decomposition, the Hilbert spectrum, the time-  
 frequency-

38 amplitude spectrum associated with each IMF<sup>j</sup>,  $H_j(\omega, t)$ , is defined as 39

$$\begin{aligned} \rightarrow & 40 \quad a(t), \omega = \omega^j \\ & 41 \quad H_j(\omega, t) = 0, \quad \text{otherwise.} \\ & (2) \end{aligned}$$

42  
 55  
 56  
 57  
 58  
 59  
 60  
 61  
 62  
 63  
 64  
 65

43 Frequencies and amplitudes are displayed separately. Negative frequencies appear  
 occasion-  
 44 ally as a result of a violation of the IMF condition. For example, a trough may occur at the  
 45 expected time but not cross zero (that is, remain positive). In the absence of a well-  
 founded  
 46 interpretation, these should be ignored. They are only reported for completeness. As  
 neces-  
 47 sary, the Marginal Hilbert Spectrum for an IMF is calculated as

$$h_{jdt}(\omega) = \frac{1}{T} \int_{1850:1}^{2021:12} H_j(\omega, t)$$

51  
52  
53  
54  
55  
56  
57  
58  
59  
60  
61  
62  
63  
64  
65

$$(3) \quad \frac{1}{172 \times 12} \int_{t=1850:1}^{2021:12} H_j(\omega, t) \approx \sum a_j(t) I(\omega = \omega_j(t)),$$

where  $I$  is the indicator function and the limits have the format year:numeric month. The  
 final, presented  $\tilde{h}_j(\omega)$  is then obtained by applying the Epanechnikov kernel smoother to  $h_j(\omega)$  for all  
 $\omega > 0$ . The smoothing turns the discontinuous  $h_j(\omega)$  into a continuous, more interpretable function. The  
 final result displays amplitude as a function of frequency, similar to a Fourier Spectrum. Only the modes  
 are analyzed, as they are invariant to expression 10 by frequency or period, unlike averages. They also  
 have the interpretation of being spectral

11 peaks.  
 12 A final concept used is the energy or power of a signal. For a signal  $y_t$ , its energy is the 13  
 integral of its squared amplitude:

$$(4) \quad e_y = \frac{1}{T} \int_0^T a_t^2(t) dt$$

16 where  $T$  is the length of  $y_t$ . Since an IMF is centered, its energy is equal to its variance. 18  
 A full analysis is provided only for the global data. Decompositions and trend analyses  
 19 only are provided for the other datasets.

20  
21  
22  
23

#### 4.1 Decompositions



24 Figure 1 displays the global median temperature anomaly for 1850-2021. Several things 25 are  
26 readily apparent. Average temperature is rising throughout the period, with sustained 26 declines  
27 during the approximate periods 1880-1910, 1940-1970 and 2000-2010. The series 27 is particularly  
28 noisy before 1900. The reduction of noise over time, especially during the  
29 satellite era, reflects better measurements.

30  
31 *4.1.1 Global* 32 33 Figure 2 displays the ICEEMDAN decomposition of median global  
34 temperature anomalies. 34 IMF 1 estimates the noise. IMFs 2-8 estimate the respective  $\phi_{ji}$  in  
35 descending order of  
36 frequency. IMF 1's amplitude is particularly high before around 1890. Figure 3 shows that  
37 IMF 1's amplitude rose to a sustained peak around the 1870s. The additional noise in IMF  
38 1 spills over into the other IMFs, especially IMFs 2 and 3, which show amplitude peaks  
39 coinciding with IMF 1's early peak. Figure 4 displays the frequencies. IMF 1 is clearly 39  
40 the noise mode with its greatest variation in frequency, ranging from near 0 to near 6, the  
41 Nyquist frequency. IMFs 2 and 3 show clustering around 2 and 1 cycle(s) per year: these are 41  
42 the semiannual and annual IMFs. IMFs 4-8 have frequencies of less than 1 per year.

43 To better understand the frequencies, Figure 5 shows the periods: the reciprocals of the 43  
44 frequencies. IMF 4 is dominated by 2 year periods. IMF 5's period fluctuates between 1 and  
45 over 20 years. IMF 6 shows a peak period of over 3300 years in 2008 in the middle of a  
46 surge from 2006 to 2011. This correspondes to a period of slowing, than decreasing decline  
47 in IMF 6. IMF 7's period generally varies between 10 and 20 with increases to around 60  
48 years and declines below 5 years. IMF 8's period generally lies between 50 and 90 years,  
49 with an increase to almost 500 in 1992. While the subsequent decline is largely  
50 explained  
51 by global warming acceleration, discussed below, its onset before acceleration is difficult  
52 to  
53 understand.  
54

55  
56  
57  
58  
59  
60  
61  
62  
63  
64  
65

1  
2  
3  
4  
5  
6  
7  
8  
9

Figure 6 shows the smoothed Marginal Hilbert Spectra for IMFs 5-8. While this Figure confirms that frequencies are decreasing, it is otherwise hard to interpret. Figure 7 displays the inverted Marginal Hilbert Spectra. The horizontal axis has the natural interpretation of being the period. IMF 5 shows a modal period of 7 years, with a positively skewed spread of 3-17 years. IMF 6's mode is 9 years, with a wider, similarly skewed spread of 7-25 years. Its uppermost year is well to the right. IMF 7 shows the most variability, with its main mode at 16-17 years, a nearly equal mode at 22 years, a major secondary mode at 37 years and a minor mode at . IMF 7's upper tail does not decay to 0 by 50 years. In fact, it remains 10 relatively high. IMF 8's period peaks at 71 years, with a small skewness of -0.13 for the

11 periods displayed. No IMF corresponds to the 11-year solar cycle. Its energy is too low to  
12 distinguish it from the noise. Table 1 shows that the multidecadal IMF 8 has the greatest  
13 energy. This, and its timing, is consistent with Wu, Huang et al. (2011) with the exception  
14 that its amplitude is even more variable. Moreover, IMF 8 accelerates beginning in  
15 1993, 15 which will be explored more in Subsection 4.2.

16  
17  
18

#### 4.1.2 Regional

19 Figures 8, 9 and 10 display the monthly average temperature anomalies and their decompo-  
20 sitions for the Northern Hemisphere, Southern Hemisphere and Tropics, respectively. With  
21 the exception of IMF 8's amplitudes, as explained in Subsubsection 4.2, they are generally  
22 similar. Table 2 shows the trend increases in the temperature anomalies, globally and region-  
23 ally. It shows two effects. First, warming is greater at higher latitudes as shown by the  
24 greater  
25 temperature increase globally compared to the Tropics when they have approximately the  
26 same share of land area: 29.2% globally and 28.6% in the Tropics.<sup>2</sup> Excluding ice-  
covered

27 surfaces from the calculation only increases this effect. Second, greater surface land area 27  
increases warming. Land covers 29.3% of the Northern Hemisphere compared to 19.1% of 28 the  
Southern Hemisphere. Again, excluding ice-covered surfaces increases this latter effect.

29  
30

#### 4.2 Global Warming Acceleration and Hiatus

31  
32

55  
56  
57  
58  
59  
60  
61  
62  
63  
64  
65

1  
2  
3  
4  
5  
6  
7  
8  
9  
33  
34  
35  
36  
37  
38  
39  
40  
41  
42  
43  
44  
45  
46  
47  
48  
49  
50  
51  
52  
53  
54

By decomposing temperatures into their constituent modes we can obtain insights into observed phenomena and new phenomena. The most important is a fuller explanation of Hansen and Oh's (2021) finding of recent global warming acceleration. We find that this warming began around 1993, which is not apparent from their graphs that show a recent, possibly temporary, increase above a linear trend. We posit that accelerating sea ice decline is the cause of global warming acceleration. We also find that the Global Warming Hiatus that first appeared in the media and Internet (Easterling and Wehner 2009) and was subsequently analyzed by many is at least mostly a mirage caused by the confluence of 41 multiannual cycles.

Figure 11 displays IMF 8 globally and for each region studied. Close examination shows a recent acceleration in the global cycle, which is harder to discern regionally. Figure 12 shows the derivative of each corresponding IMF 8 with respect to time. In each geography, IMF 8 is sinusoidal with varying amplitudes and a 50-year period. However, the first peak corresponds to a flatter, declining period in the Tropics. The derivative of global IMF 8 presents a point of inflection in 1993, which leads to a slowing of the rate of temperature 48 increase, then accelerating increase. The regional graphs are more subtle. Each derivative of 49 \_\_\_\_\_

<sup>2</sup> I'd like to thank D.W. Rowlands for calculating the latter figure.

IMF 8 is sinusoidal (except, of course, the Tropics before around 1900) until 1993 when, outside of the Southern Hemisphere, they turn into roughly straight lines above the expected continuations of the sinusoids. The Northern Hemisphere has an accelerating temperature increase, while the Tropics has a decelerating decrease. These are all equivalent to, and contributing to global temperature warming acceleration. The weakness or absence of the acceleration in the Southern Hemisphere may indicate more specifically that it is the decline in Northern sea ice that is driving acceleration. Hansen and Oh (2021) extrapolate a linear approximation of a 132 running mean of global temperatures, 1970-2015, to find that tem<sub>10</sub> peratures afterwards are above expectation. They conclude that global warming acceleration

55  
56  
57  
58  
59  
60  
61  
62  
63  
64  
65

1  
2  
3  
4  
5  
6  
7  
8  
9  
11 began in 2015 based on Loeb, Johnson et al.'s (2021) interpretation of CERES (Clouds and  
12 the Earth's Radiant Energy System) satellite data. Instead, we propose that increasing loss  
13 of sea ice has been causing global warming acceleration. Sea ice is an excellent  
14 candidate because ice reflects more sunlight than seawater. Thus, its loss increases  
global warming.

15 beyond that caused by any other forcings (Dai, Luo et al. 2019). According to National  
16 Snow and Ice Data Center (2020) Figure "Mean sea ice anomalies, 1953-2018," Northern  
17 Hemispheric sea ice started declining around 1988 with evidence of acceleration.

18 Figure 13 shows the sum of the multiannual median IMFs 5-8, and residual trend. The  
19 cooling period during the 2000s now appears. It is clear that this global warming hiatus,  
20 originally analyzed by Easterling and Wehner (2009), occurred as a result of the  
multiannual  
21 cycles corresponding to IMFs 5-7 being in declining phases, even while IMF 8, the most  
22 energetic IMF, was increasing. When these cycles resumed increasing, the cooling  
period ended. IMF 7 peaks around 2000, though it alone is not enough to account  
23 for the pause due 24 to its low amplitude.

## 25 26 27 5 Discussion

28  
29 We have used ICEEMDAN to decompose the Met Office Hadley Centre's median  
monthly

30 temperature anomaly into noise, cycles and a residual trend. Our most important  
finding is<sup>3</sup>The global cooling hiatus of the early

31 global warming acceleration beginning around 1993,

32 2000s is coincidental, being the result of cyclic downturns.

33 The multidecadal cycle with a period of 50 years is responsible for global warming accel-  
34 eration. We hypothesize that this is due to accelerating sea ice loss, which is  
documented

1  
2  
3  
4  
5  
6  
7  
8  
9  
35 to have begun around 1988, two decades earlier than the start of Hansen and Sato's  
(2021) <sup>36</sup> claim. This is supported by Hugonnet, McNabb et al. (2021), who find that  
global glacier ice

37 mass loss has been accelerating during 2000-2019, providing confirmation of global warm-  
<sup>4</sup>These three accelerations suggest some sort of linkage.  
38 ing acceleration during this period.

39 Hu Hansen and Sato (2021) use linear regression to produce a smooth trend for the global<sup>5</sup>  
This is based on the 132 month running mean,  
40 average temperature anomaly, 1970-2015.  
41 which appears close to linear, during 1970-2015. They then find that the global  
temperature  
42 anomaly after 2015 is completely above this trend. They hypothesize that this is due to  
in<sup>43</sup> creased atmospheric aerosols increasing temperature forcing, leading to  
accelerated global <sup>44</sup> warming. However, lacking information about temperature cycles,  
they cannot determine  
45 whether they are truly observing acceleration, a temporary or permanent change in  
trend or  
46 an anticipable peak in an underlying cycle. Their inability to precisely identify whatever  
they

---

47 <sup>3</sup> Due to estimation error, the precise timing is unavailable. Fortunately, this error is in the range of  
months.

48 <sup>4</sup> Glacier ice mass loss is linearly proportionate to local temperature increase (Hugonnet, McNabb et al.  
<sup>49</sup> 2021). Accelerating loss can only be caused by accelerating increase. <sup>50</sup> <sup>5</sup> Unfortunately, Hansen  
and Sato (2021) do not cite their data source.

51  
52  
53  
54 found precludes policy prescriptions. Instead, our evidence provides actionable  
information: Sea ice restoration should be a part of global warming mitigation. IMF 8's  
early Tropical nonappearance and early weak appearance at other latitudes is worthy of  
investigation.

55  
56  
57  
58  
59  
60  
61  
62  
63  
64  
65

1  
2  
3  
4  
5  
6  
7  
8  
9

The global cooling pause has a simple explanation in decreases in global multiannual cycles, which can be seen individually in Figure 2. IMFs 5-8 and in their sum including the residual trend in Figure 13. Each of these IMFs has a particularly low trough after 2000, consistent with a negative forcing. Ridley, Solomon et al. (2014) provide evidence for this forcing in the form of increased and variable stratospheric volcanic aerosols. Coincidence 10 with a modal trough can lower that trough. Militating against this is the accelerating global 11 glacier ice loss during this period. The increased CO<sub>2</sub> uptake of Keenan, Prentice et al. 12 (2016) and the similar increased photosynthesis hypothesis of Leggett and Ball (2015) have to 13 be rejected because these would have been reflected in sustained decreases in low frequency 14 IMFs in the ICEEMDAN decompositions.

15 The first three cycles have clear physical interpretations. The semiannual and annual  
16 cycles (IMFs 2 and 3) capture the seasonal variations in average temperature driven by  
17 changes in absorbed insolation. The biennial cycle reflects the Quasi-Biennial  
Oscillation 18 possibly interacted with other phenomena with approximately biennial  
cycles.

19 Pooling observations, in this case, 5° by 5° latitude-longitude cells, reduces the relative  
20 noise, thus increasing identifiability of cycles and trends. As is visible in the early  
decades of

21 the series, noise can spillover into low frequency cycles. As the noise increases,  
increasingly

22 lower frequency cycles can become unidentifiable. Moreover, except for the very  
lowest

23 frequency cycle, the lowest frequencies have the least energy per Table 1. Their low  
energies 24 are additional impediments to their identification in the presence of  
noise. Thus, EMD and

25 its derivatives have to be used on temperature series that have pooled enough  
observations to

26 reduce noise to a manageable level. It may be possible to use a spatiotemporal  
generalization

27 of EMD on a grid, provided that the spatial structure enables canceling enough noise to

28 improve identifiability. Coarser grids may accomplish this at the potential risk of producing

55  
56  
57  
58  
59  
60  
61  
62  
63  
64  
65

1  
2  
3  
4  
5  
6  
7  
8  
9  
29  
32  
33  
34  
36  
37  
38  
39  
40  
41  
43  
44  
45  
46  
47  
48  
49  
50  
51  
52  
53  
54

too little spatial detail. An improved version of the spatial EMD of Fauchereau, Pegram, and Sinclair (2008) may be able to do this. A requirement is the ability to draw strength across space to reduce noise.

## 6 Conclusions and Extensions 35

Understanding multiannual temperature cycles can shed new light on the climate in general.

The global warming acceleration that began in 1993 is only visible in the multidecadal cycle. This acceleration is proposed to be due to accelerating sea ice loss beginning around 1988, particularly in the Northern Hemisphere. This improves on Hansen and Sato's (2021) claimed recent global warming acceleration based on extrapolating a trend. By using cyclical information, we have avoided the biases from not accounting for cyclical information when forecasting. Moreover, we have pinpointed, within estimation variation, the beginning

of this acceleration. The strongest evidence of global warming acceleration lies in accelerating global glacial ice mass loss during 2000-2019. Confirmatory research is needed to verify that sea ice loss has indeed been accelerating and to fully incorporate Southern Hemispheric sea ice loss into explanations of global temperature warming acceleration. The policy implication is clear: sea ice restoration is a necessary part of global warming mitigation.

The Global Warming Hiatus has been shown to be, at most, the effect of volcanic forcings. It may very well have been a mirage. Again, this was only made possible by decom-

posing global temperature changes into their underlying trend and cycles. The Hiatus had

55  
56  
57  
58  
59  
60  
61  
62  
63  
64  
65

| IMF | Energy * 1000 |
|-----|---------------|
| 1   | 3.8           |
| 2   | 2.1           |
| 3   | 2.3           |
| 4   | 2.9           |
| 5   | 2.6           |
| 6   | 2.2           |
| 7   | 1.4           |
| 8   | 8.0           |

2 Table 2 Temperature Anomaly Residual Trend Changes

| Region              | Degrees Celsius |
|---------------------|-----------------|
| Global              | 0.76            |
| Northern Hemisphere | 0.92            |
| Southern Hemisphere | 0.58            |
| Tropics             | 0.62            |

3 minimal, if any, effect on global glacial ice mass loss. Accelerating global glacial ice loss provides  
4 evidence against the hiatus.

5 ICEEMDAN, the technique we used, is superior to EMD and EEMD, the previous EMD-  
6 based methods to analyze global temperature changes due to its ability to handle noise,  
7 output informative IMFs in decreasing order of frequency and reduction of residual IMFs.  
8 All of these techniques share the advantages of being data-driven, having minimal  
9 assumptions and being applicable to almost any kind of time series. In particular, they do  
10 not require assuming particular functional forms for the cycles or trends. They can be used  
11 to improve climate models by identifying temperature and other cycles with variable  
12 amplitudes and frequencies. Even the estimated noise can inform these models. It may be  
13 possible to develop a spatial method that accounts for spatial correlations and draws  
14 strength across space to provide local EMD-style decompositions.<sup>1</sup> These can provide local  
15 information to better improve climatic understanding and inform climate models.

16 Acknowledgements I'd like to thank D.W. Rowlands for calculating the Tropical surface water percentage,  
17 the Met Office Hadley Centre for providing me with the Tropical data series and an anonymous referee for  
18 helpful comments.

## 19 Availability of data and material

20 Global and hemispheric source data are from the Met Office Hadley Centre observations datasets  
21 at  
22 <https://www.metoffice.gov.uk/hadobs/hadcrut5/data/current/download.html>, downloaded  
23 February 17, 2022. Tropical data are from a file emailed by the Met Office Hadley Centre on  
24 the same date. All data are included in the supplemental materials.

<sup>1</sup> Fauchereau, Pegram, and Sinclair (2008) is a first step in this direction.



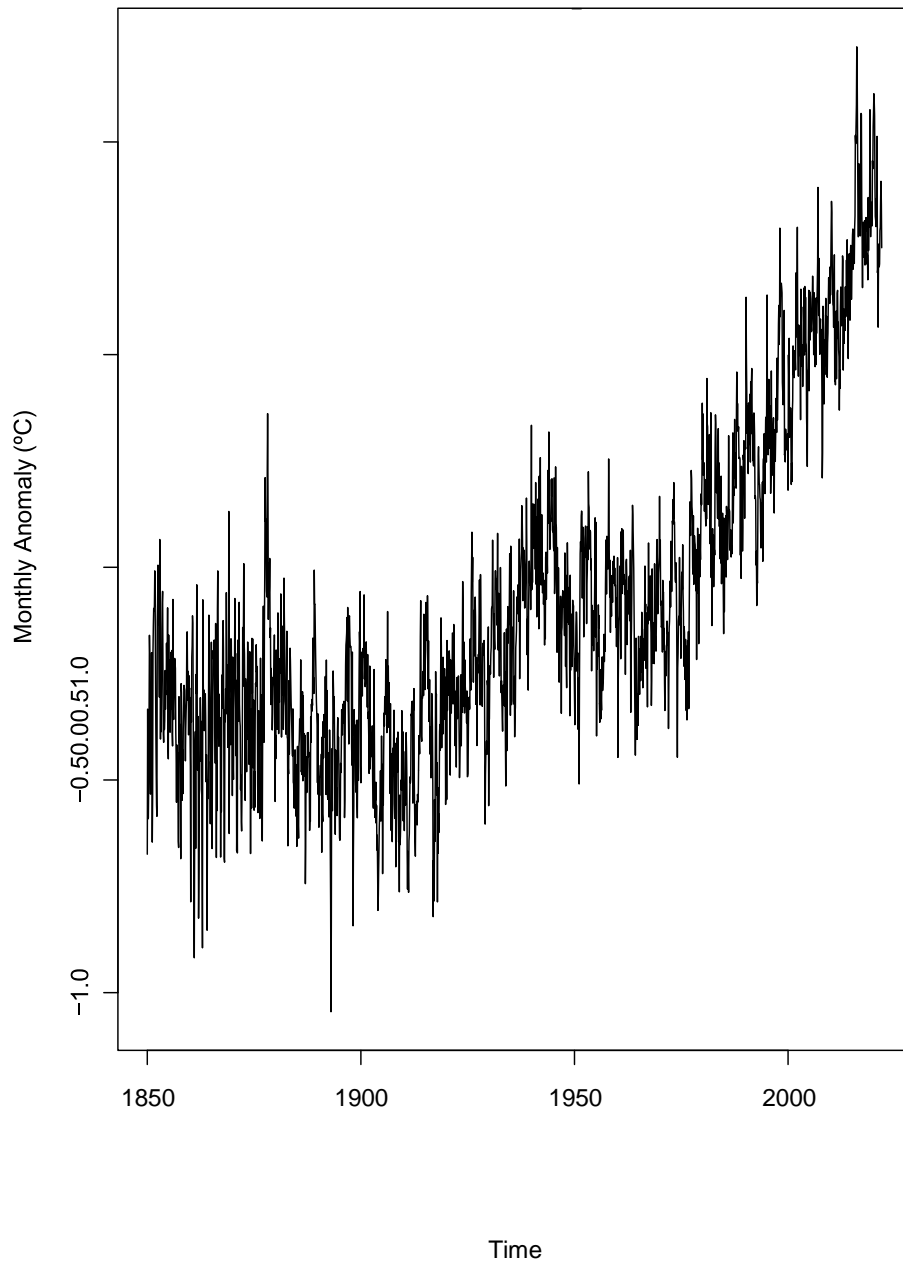
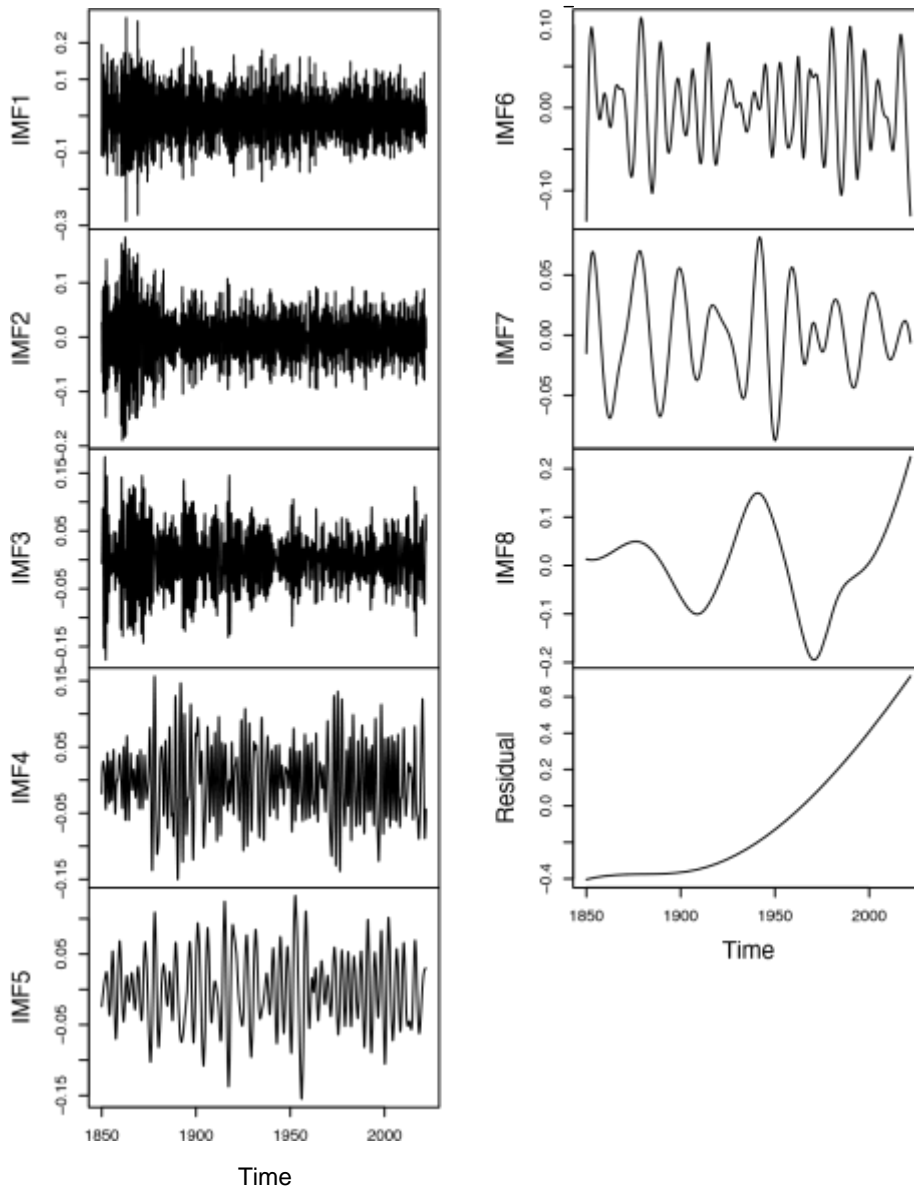


Fig. 1 Mean Average Global Temperature Anomalies, 1850-2021

56  
57  
58  
59  
60  
61  
62  
63  
64  
65



1

2

3 Fig. 2 ICEEMDAN Decomposition of Mean Average Global Temperature Anomalies (°C), 1850-2021

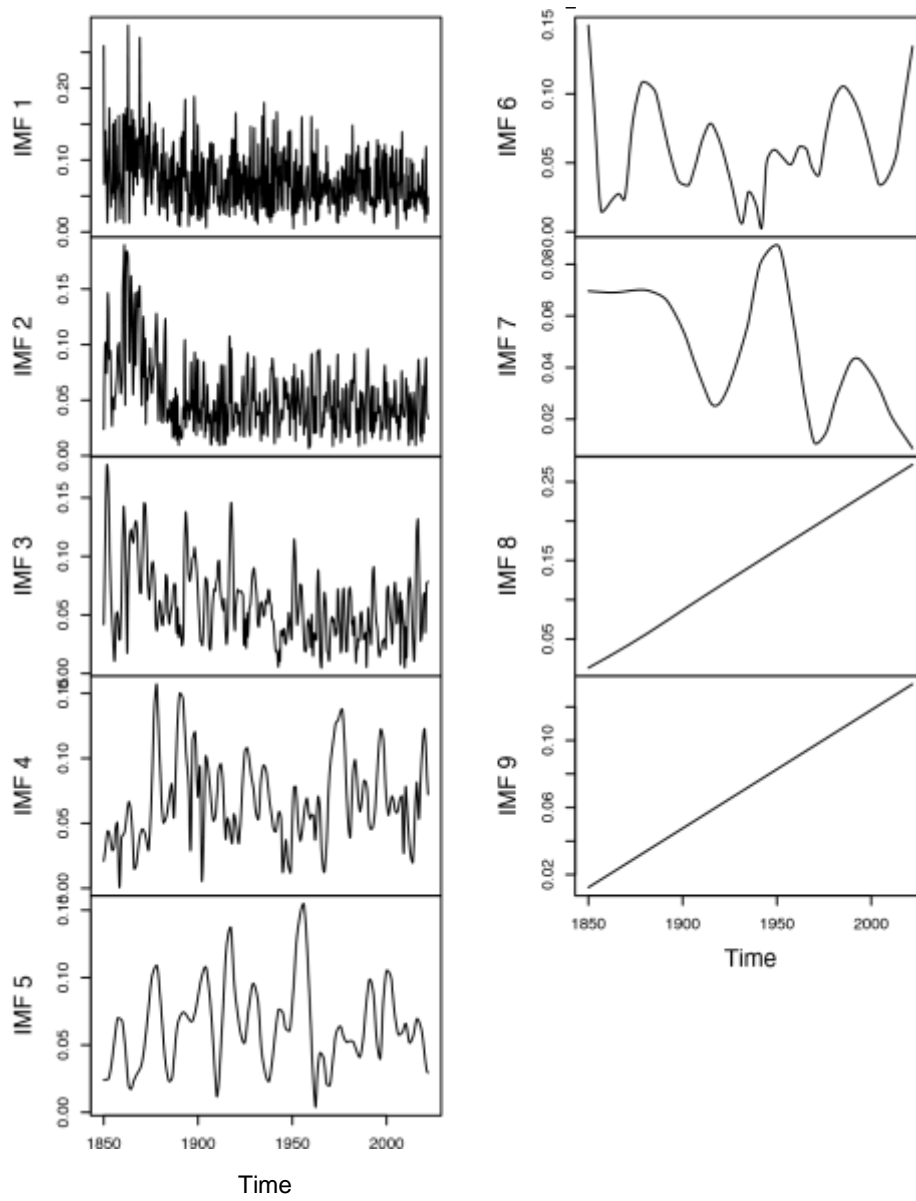
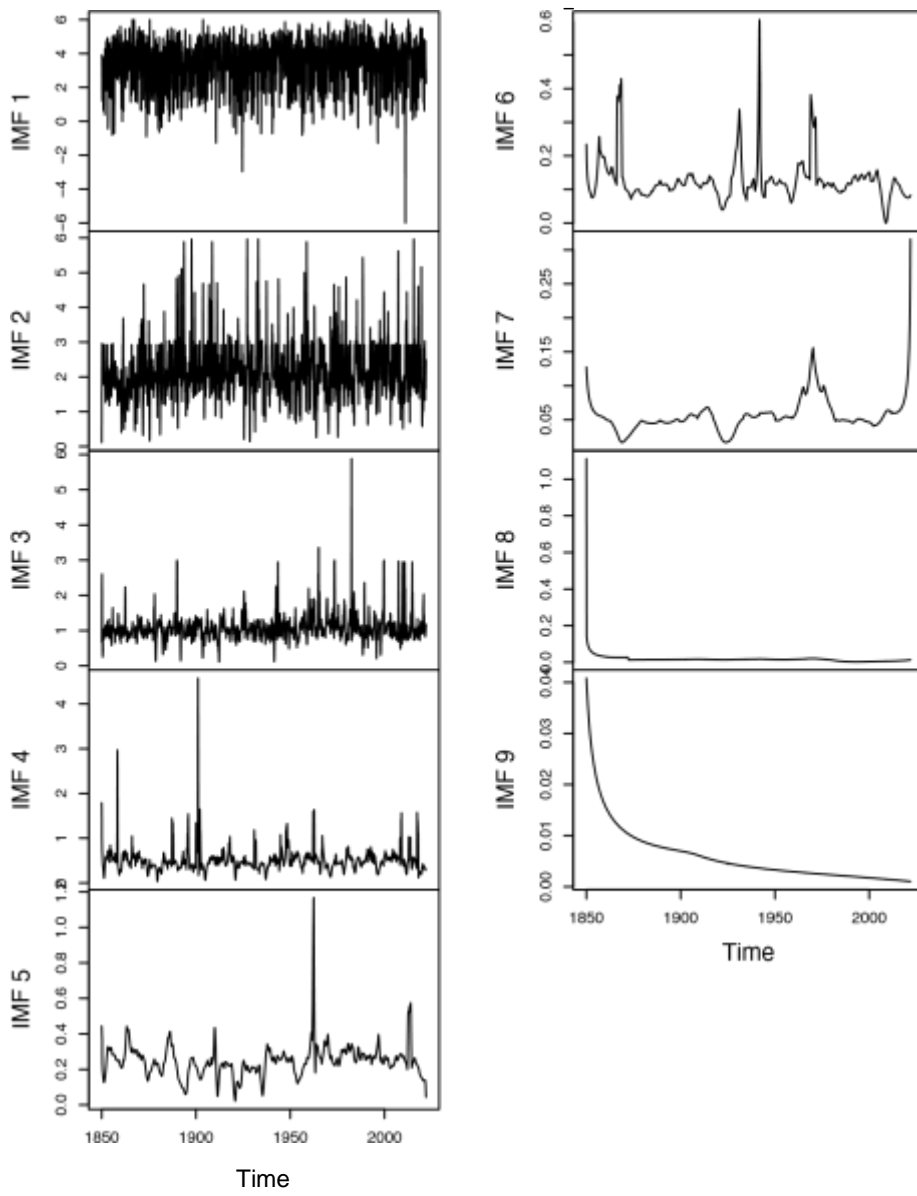


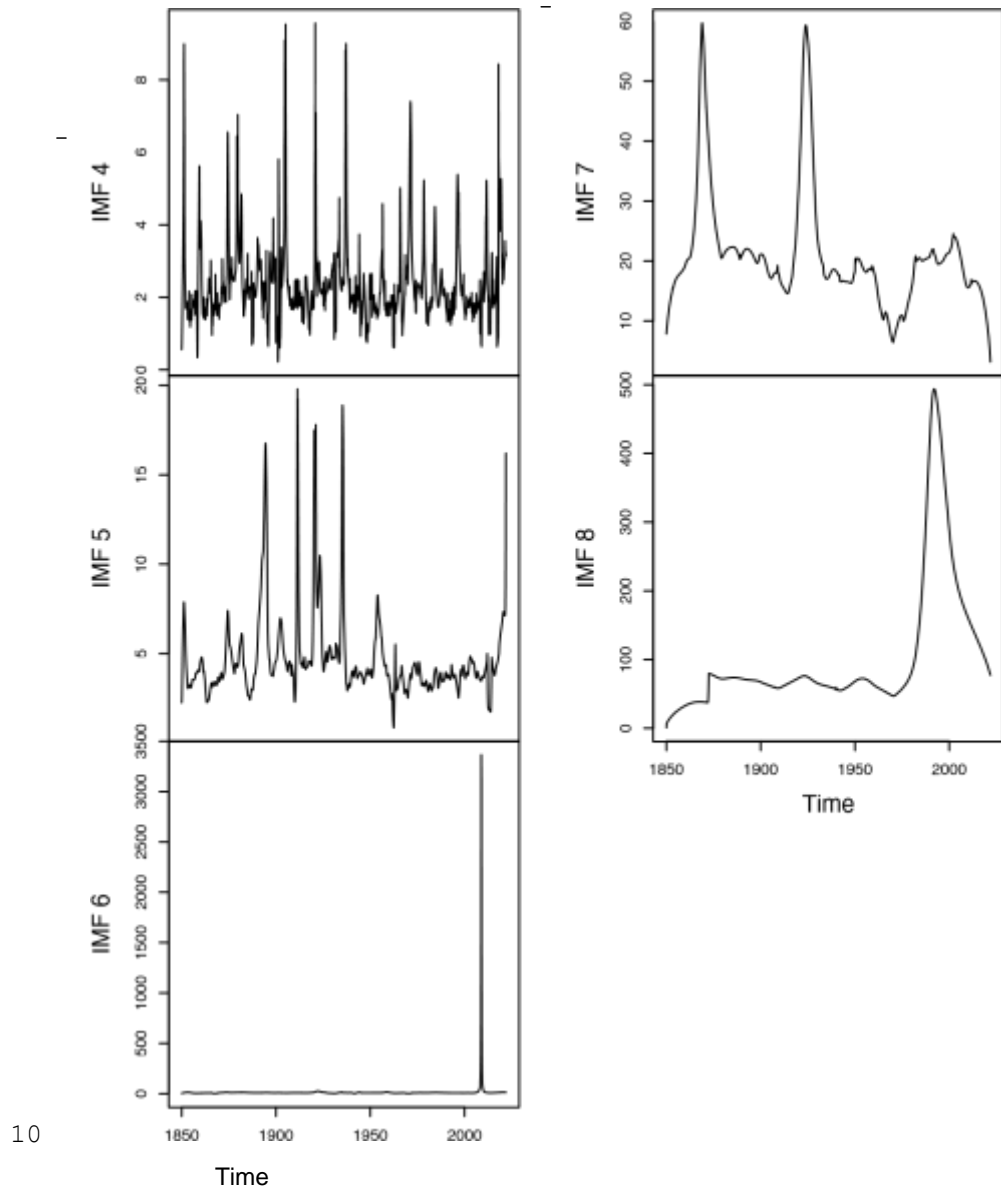
Fig. 3 Amplitudes of Mean Average Global Temperature Anomalies IMFs ( $^{\circ}\text{C}$ ), 1850-2021



7

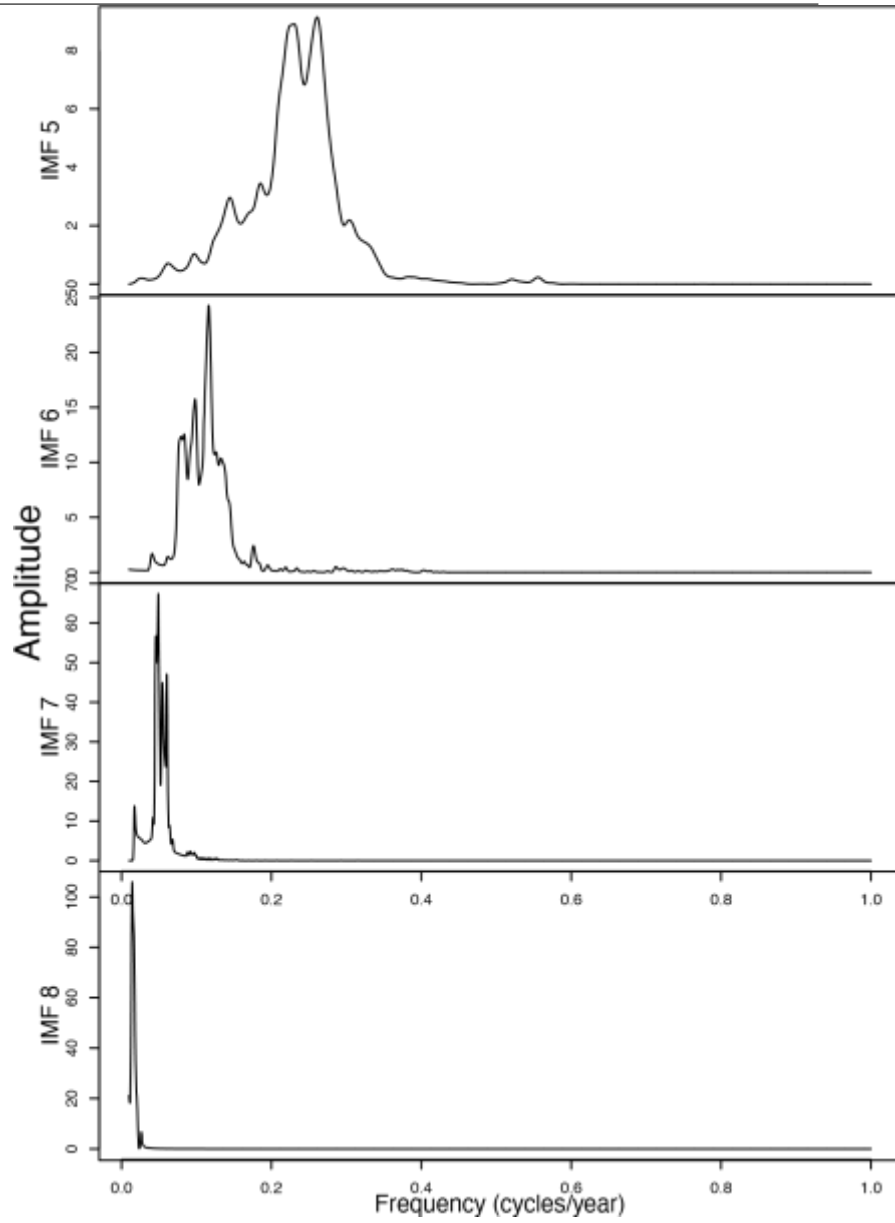
8

9 Fig. 4 Frequencies of Mean Average Global Temperature Anomalies IMFs (cycles/year), 1850-2021



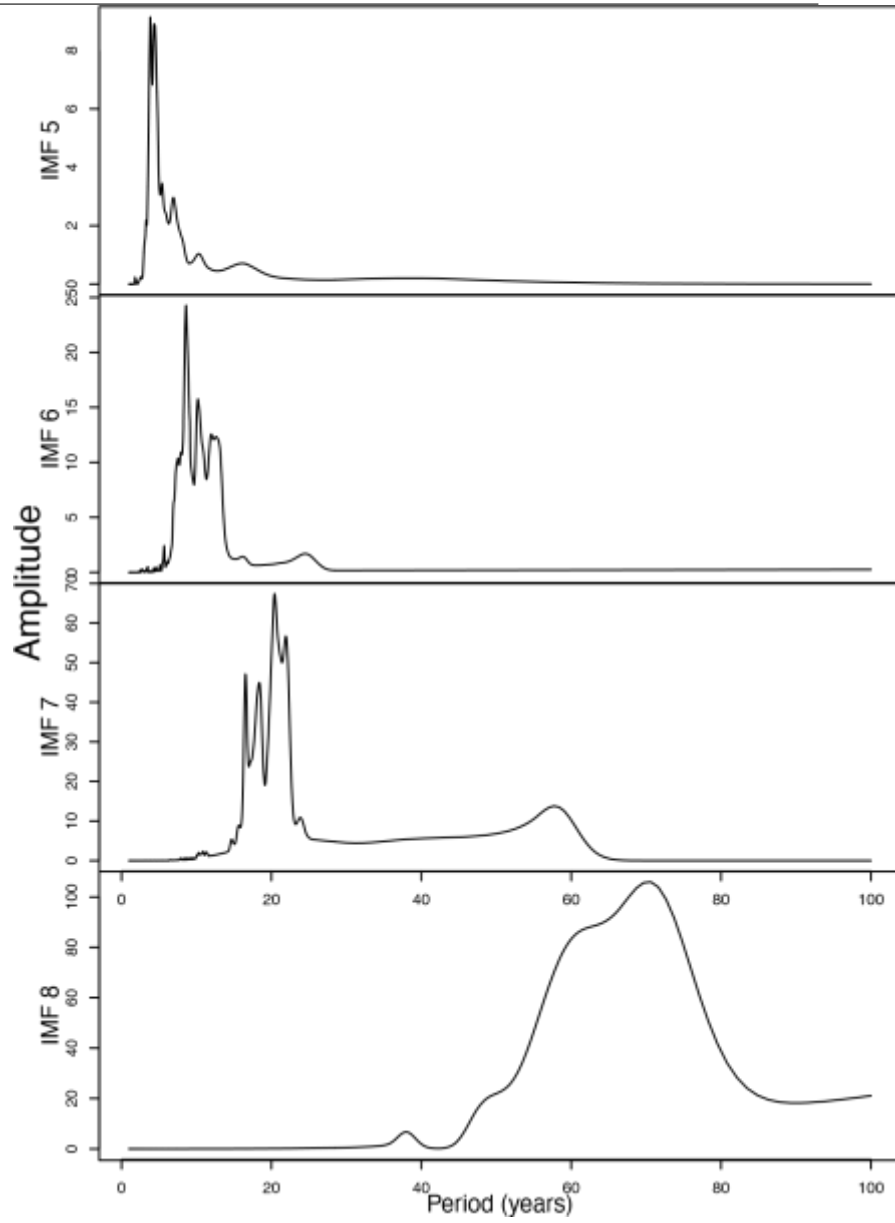
10  
11

12 Fig. 5 Periods of Mean Average Global Temperature Anomalies, IMFs 4-8 (years), 1850-2021



13

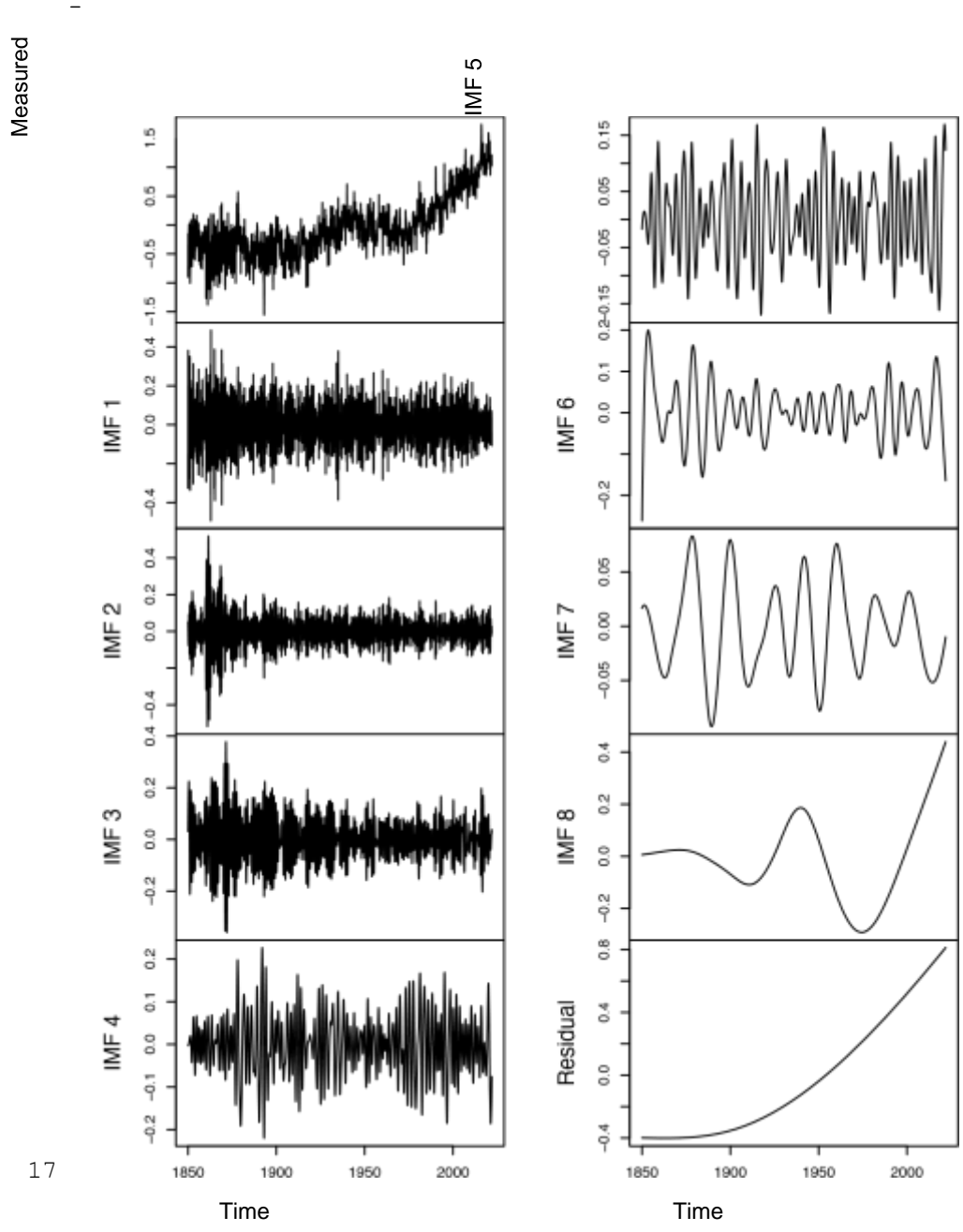
14 Fig. 6 Marginal Hilbert Spectra, IMFs 5-8



15

16 Fig. 7 Inverted Marginal Hilbert Spectra, IMFs 5-8

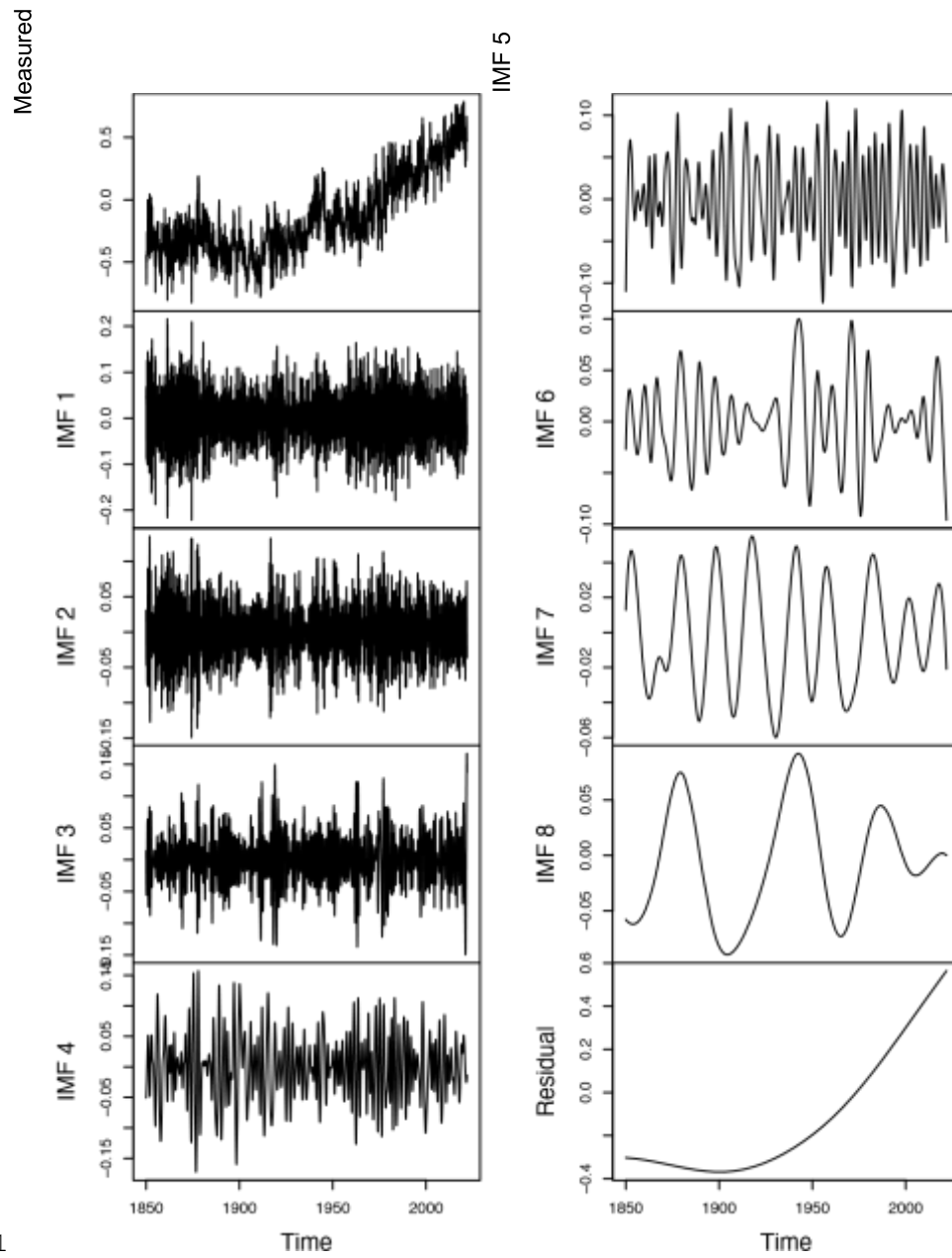




17

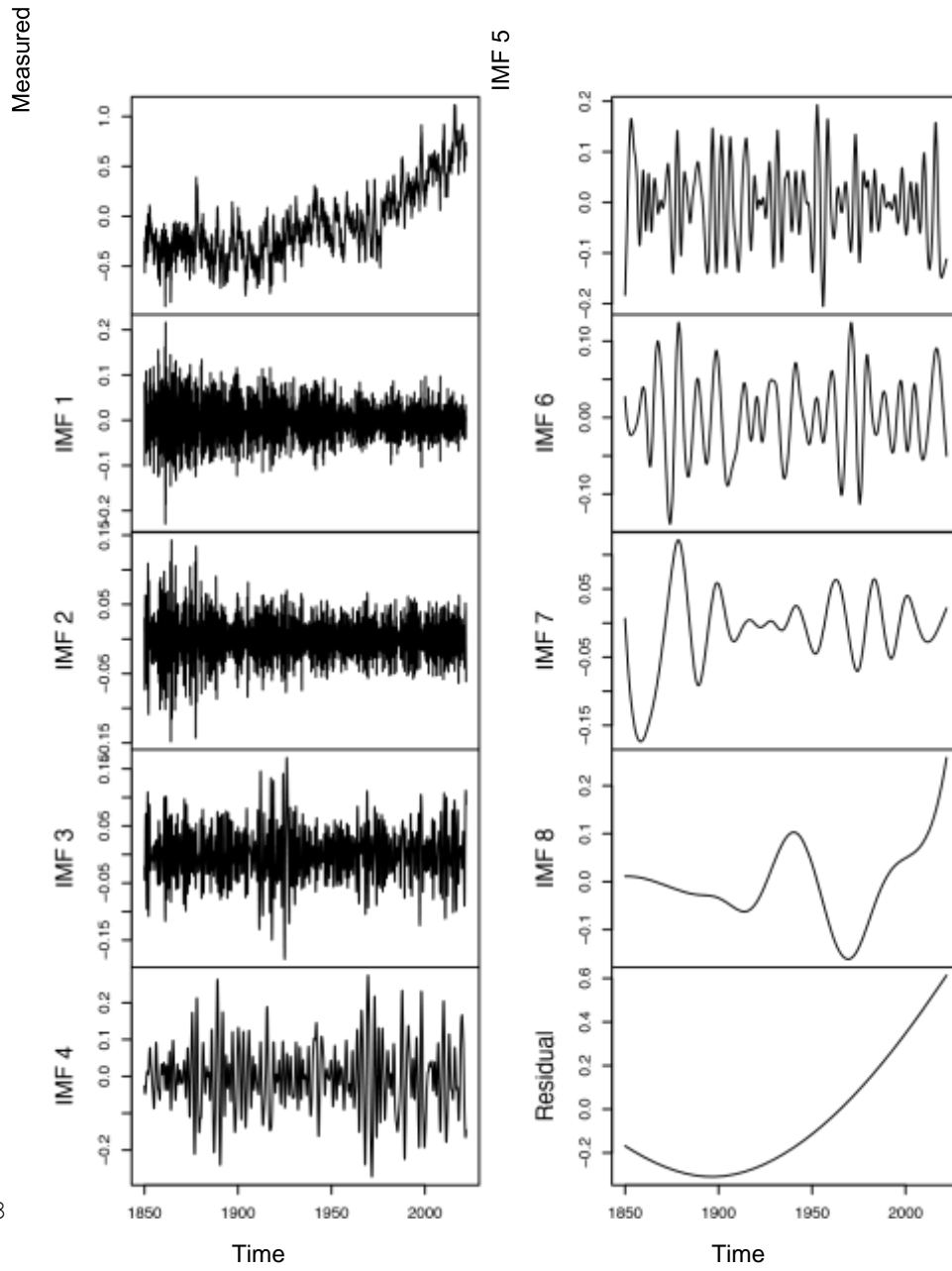
18

19 Fig. 8 Average Mean Northern Hemisphere Temperature Anomalies with ICEEMDAN Decomposition (°C),  
20 1850-2021



21

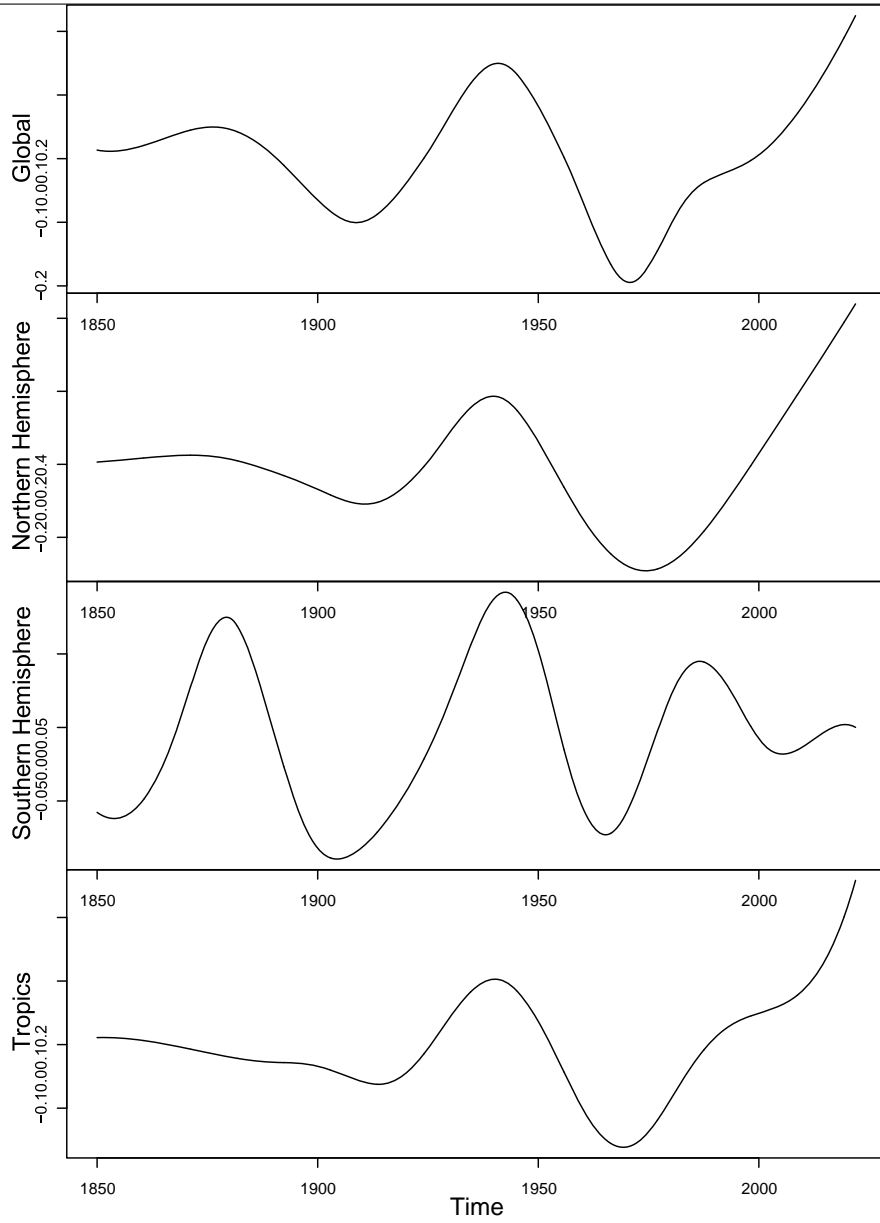
22 Fig. 9 Average Mean Southern Hemisphere Temperature Anomalies with ICEEMDAN Decomposition (°C), 1850-2021



23

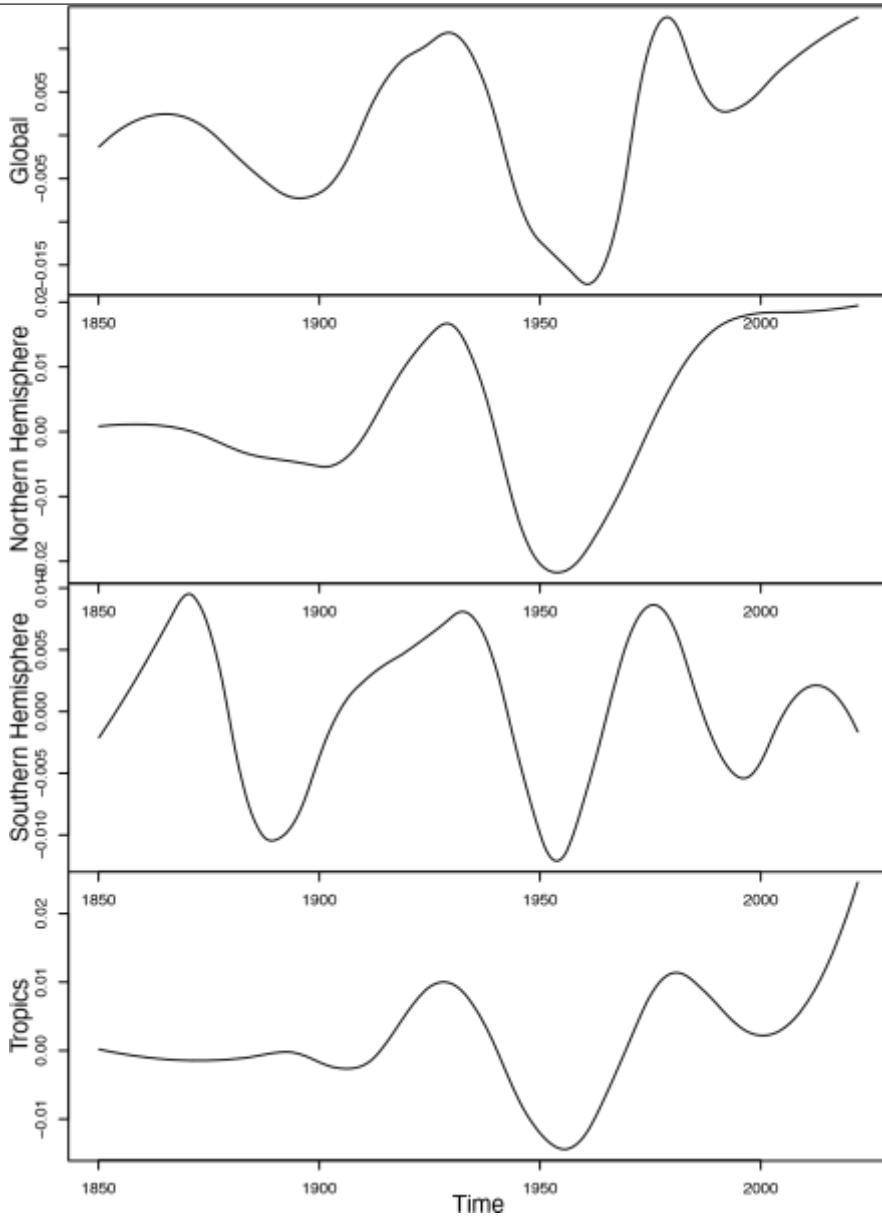
24

25 Fig. 10 Average Mean Tropical Temperature Anomalies with ICEEMDAN Decomposition (°C), 1850-2021



26

27 Fig. 11 IMF 8, Globally and Regionally (°C), 1850-2021



28

29 Fig. 12 First Derivative of IMF 8, Globally and Regionally (°C), 1850-2021

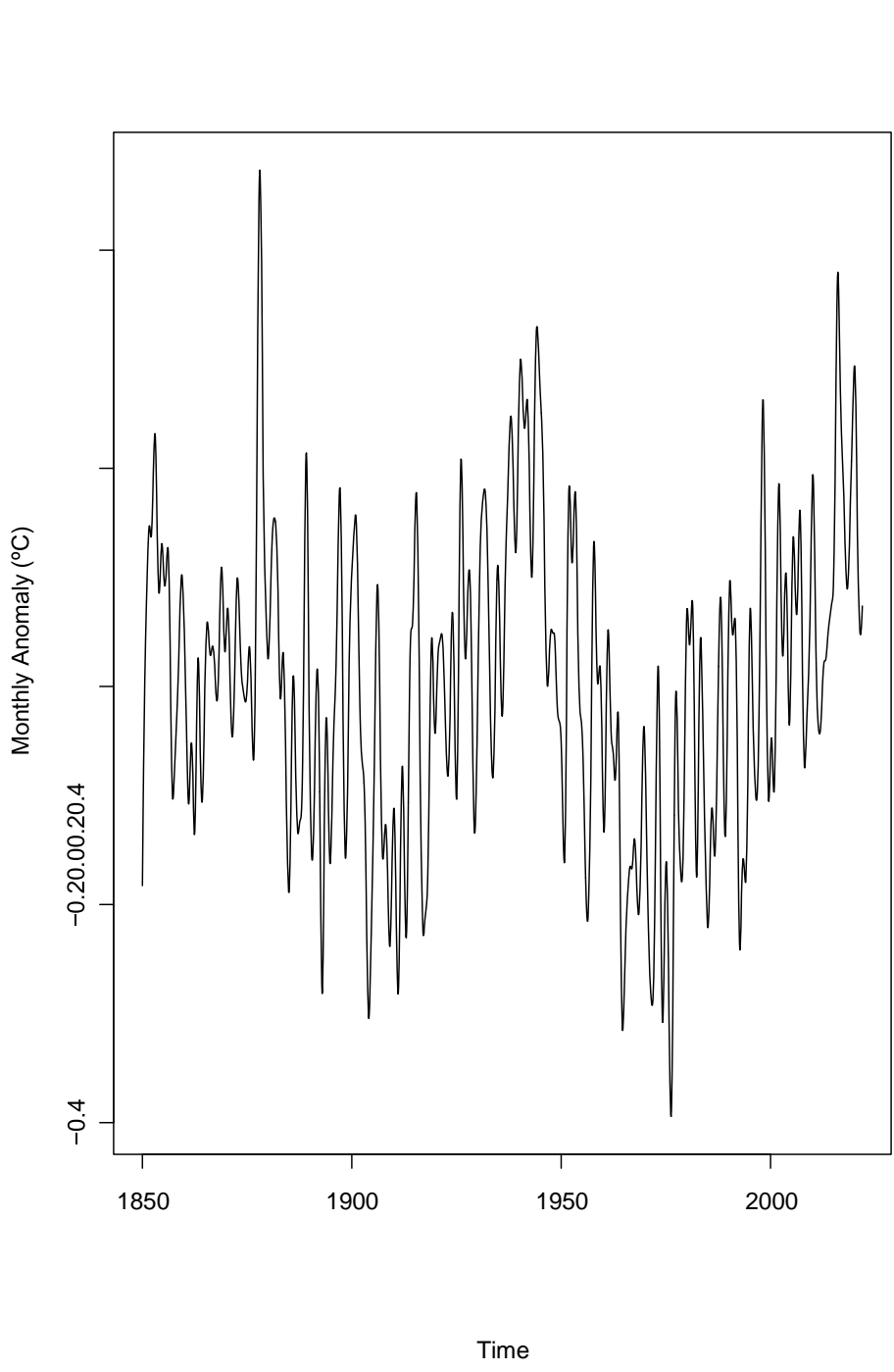


Fig. 13 Sum of Global IMFs 5-8 and Residual (°C), 1850-2021

56  
57  
58  
59  
60  
61  
62  
63  
64  
65

#### Code availability

3 All programming was done in R. The R programs and workspace file are included in the 4  
5 supplemental materials.

6  
7  
8

#### Author's Contribution

9  
10 The author declares that he is the sole author of this work.

11  
12  
13

#### Author Declarations

14  
15 Not applicable.

16  
17  
18

#### Funding

19  
20 Not applicable.

21  
22  
23

#### Conflict of interest

24  
25 The author declares that he has no conflict of interest.

26  
27  
28

#### References

- 29  
30 Bjornsson H, Venegas SA (2000) A manual for EOF and SVD analyses of climate data." 31  
Tech. rep., McGill University, Montreal, Quebec, Canada, URL [http://muenchow. 32](http://muenchow.cms.udel.edu/classes/MAST811/eof.pdf)  
[cms.udel.edu/classes/MAST811/eof.pdf](http://muenchow.cms.udel.edu/classes/MAST811/eof.pdf)  
33 Bretherton CS, Widmann M, Dymnikov VP, Wallace JM, Blade I (1999) The effective num34 ber of  
spatial degrees of freedom of a time-varying field. *Journal of Climate* 12:1990–  
35 2009  
36 Colominas MA, Schlotthauer G, Torres ME (2014) Improved complete ensemble EMD: A  
37 suitable tool for biomedical signal processing. *Biomedical Signal Processing and*  
38 *Control* 14:19–29, DOI <https://doi.org/10.1016/j.bspc.2014.06.009>  
39 Dai A, Luo D, Song M, Liu J (2019) Arctic amplification is caused by sea-ice loss un40 der increasing  
CO<sub>2</sub>. *Nature Communications* 10(1):121, DOI <https://doi.org/10.1038/>  
41 [s41467-018-07954-9](https://doi.org/10.1038/s41467-018-07954-9)

- 42 Deering R, Kaiser J (2005) The use of a masking signal to improve empirical mode de43  
composition. In: Proceedings. (ICASSP '05). IEEE International Conference on Acous44  
tics, Speech, and Signal Processing, 2005., vol 4, pp iv/485 – iv/488 Vol. 4, DOI  
45 <https://doi.org/10.1109/ICASSP.2005.1416051>
- 46 Easterling DR, Wehner MF (2009) Is the climate warming or cooling? Geophysical Re47  
search Letters 36:L08706, DOI <https://doi.org/10.1029/2009GL037810>
- 48 Fauchereau N, Pegram G, Sinclair S (2008) Empirical mode decomposition on the sphere: 49  
application to the spatial scales of surface temperature variations. Hydrology and Earth  
50 System Sciences 12:1–9, DOI <https://doi.org/10.5194/hess-12-933-2008> 51  
52  
53  
54  
55  
56  
57  
58  
59  
60  
61  
62  
63  
64  
65



- 1 Feldstein SB (2002) The recent trend and variance increase of the annular mode. *Journal*  
2 *of Climate* 15:88–94
- 3 Foster G, Rahmstorf S (2011) Global temperature evolution 1979–2010. *Environmental*  
4 *Research Letters* 6(4):044022, DOI <https://doi.org/10.1088/1748-9326/6/4/044022>
- 5 Franzke C (2010) Long-range dependence and climate noise characteristics of antarctic  
6 temperature data. *Journal of Climate* 23(22):6074–6081, DOI [https://doi.org/10.1175/](https://doi.org/10.1175/2010jcli3654.1)  
7 2010jcli3654.1
- 8 Hansen J, Sato M (2021) July temperature update: Faustian payment comes due. URL  
9 [http:](http://www.columbia.edu/~mhs119/Temperature/Emails/July2021.pdf)  
10 [//www.columbia.edu/~mhs119/Temperature/Emails/July2021.pdf](http://www.columbia.edu/~mhs119/Temperature/Emails/July2021.pdf)
- 11 Hansen J, Sato M, Ruedy R, Lo K, Lea DW, Medina-Elizade M (2006) Global temperature  
12 change. *Proceedings of the National Academy of Sciences* 103(39):14288–14293, DOI  
13 <https://doi.org/10.1073/pnas.0606291103>
- 14 Hansen J, Sato M, Ruedy R (2013) Global temperature update through 2012. URL [https:](https://www.nasa.gov/pdf/719139main/_2012_GISTEMP_summary.pdf)  
15 [//www.nasa.gov/pdf/719139main/\\_2012\\_GISTEMP\\_summary.pdf](https://www.nasa.gov/pdf/719139main/_2012_GISTEMP_summary.pdf)
- 16 Huang NE, Shen Z, Long SR, Wu MC, Shih HH, Zheng Q, Yen NC, Tung CC, Liu  
17 HH (1998) The Empirical Mode Decomposition and the Hilbert spectrum for nonlinear  
18 and non-stationary time series analysis. *Proceedings of the Royal Society of London A*  
19 454(1971):903–995
- 20 Huang NE, WU Z, Pinzon JE, Parkinson CL, Long SR, Blank K, Gloersen P, Chen X (2009)  
21 Reductions of noise and uncertainty in annual global surface temperature anomaly data.  
22 *Advances in Adaptive Data Analysis* 1(3):447–460
- 23 Hugonnet R, McNabb R, Berthier E, Menounos B, Nuth C, Girod L, Farinotti D, Huss M,  
24 Dussaillant I, Brun F, Kaˆab A (2021) Accelerated global glacier mass loss in the early  
25 twenty-first century. *Nature* 592(7856):726–731, DOI [https://doi.org/10.1038/](https://doi.org/10.1038/s41586-021-03436-z)  
26 021-03436-z
- 27 Keenan TF, Prentice IC, Canadell JG, Williams CA, Wang H, Raupach M, Collatz GJ (2016)  
28 Recent pause in the growth rate of atmospheric CO<sub>2</sub> due to enhanced terrestrial carbon  
29 uptake. *Nature Communications* 7(13428), DOI <https://doi.org/10.1038/ncomms13428>
- 30 Kim D, Kim KO, Oh HS (2012) Extending the scope of empirical mode decomposition by  
31 smoothing. *Journal on Advances in Signal Processing* 2012(168)
- 32 Lau KM, Weng H (1999) Interannual, decadal–interdecadal, and global warming signals in  
33 sea surface temperature during 1955–97. *Journal of Climate* 12(5):1257–1267, DOI  
34 [https://10.1175/1520-0442\(1999\)012<textless1257:idiagw<textgreater2.0.co;2](https://10.1175/1520-0442(1999)012<textless1257:idiagw<textgreater2.0.co;2)
- 35 Lean JL, Rind DH (2008) How natural and anthropogenic influences alter global and regional  
36 surface temperatures: 1889 to 2006. *Geophysical Research Letters* 35(18), DOI  
37 <https://doi.org/10.1029/2008gl034864>
- 38 Leggett LMW, Ball DA (2015) Granger causality from changes in level of atmospheric CO<sub>2</sub>  
39 to global surface temperature and the El Niño–Southern Oscillation, and a candidate  
40 mechanism in global photosynthesis. *Atmosphere Chemistry and Physics* 15(20):11571–  
41 11592, DOI <https://doi.org/10.5194/acp-15-11571-2015>
- 42 Lindsey R, Dahlman L (2020) Climate change: Global temperature.  
43 URL [https://www.climate.gov/news-](https://www.climate.gov/news-features/understanding-climate/climate-change-global-temperature)  
44 [features/understanding-climate/](https://www.climate.gov/news-features/understanding-climate/climate-change-global-temperature) climate-change-global-  
45 temperature

- 46 Loeb NG, Johnson GC, Thorsen TJ, Lyman JM, Rose FG, Kato S (2021) Satellite and ocean  
47 data reveal marked increase in earth's heating rate. *Geophysical Research Letters*  
48 48(13):e2021GL093047, DOI <https://doi.org/10.1029/2021GL093047>
- 49 McCloskey D, Ziliak S (2008) *The Cult of Statistical Significance*. University of Michigan  
50 Press, DOI <https://doi.org/10.3998/mpub.186351>
- 51 Morice C, Kennedy J, Rayner N, Winn J, Hogan E, Killick R, Dunn R, Osborn T, Jones P,  
52 Simpson I (in press) An updated assessment of near-surface temperature change from  
53 1850: The HadCRUT5 dataset. *Journal of Geophysical Research (Atmospheres)* DOI  
54 <https://doi.org/10.1029/2019JD032361>
- 55 Mukherjee S, Joshi R, Prasad RC, Vishvakarma SCR, Kumar K (2014) Summer monsoon  
56 rainfall trends in the Indian Himalayan region. *Theoretical and Applied Climatology*  
57 121(3-4):789–802, DOI <https://doi.org/10.1007/s00704-014-1273-1>
- 58 National Snow and Ice Data Center (2020) SOTC: Sea ice
- 59 Qian C (2015) On trend estimation and significance testing for non-gaussian and serially  
60 dependent data: quantifying the urbanization effect on trends in hot extremes in the  
61 megacity of shanghai. *Climate Dynamics* 47(1-2):329–344, DOI <https://doi.org/10.1007/s00382-015-2838-0>
- 62
- 63 R Core Team (2020) *R: A Language and Environment for Statistical Computing*. R  
64 Foundation for Statistical Computing, Vienna, Austria, URL [https://www.R-](https://www.R-project.org/)  
65 [project.org/](https://www.R-project.org/)
- 66 Ridley DA, Solomon S, Barnes JE, Burlakov VD, Deshler T, Dolgii SI, Herber AB, Nagai T, III  
67 RRN, Nevzorov AV, Ritter C, Sakai T, Santer BD, Sato M, Schmidt A, Uchino O, Vernier JP  
68 (2014) Total volcanic stratospheric aerosol optical depths and implications for global  
69 climate change. *Geophysical Research Letters* 41(22):7763–7769, DOI <https://doi.org/10.1002/2014GL061541>
- 70
- 71 Sabzehee F, Nafisi V, Iran Pour S, Vishwakarma BD (2019) Geospatial conference 2019 –  
72 joint conferences of SMPR and GI research. In: *The International Archives of the*  
73 *Photogrammetry, Remote Sensing and Spatial Information Sciences, Analysis of the*  
74 *precipitational climate signal using Empirical Mode Decomposition (EMD) over the*  
75 *Caspian catchment area, vol XLII-4/W18, pp 923–929, DOI [https://10.5194/](https://10.5194/isprs-archives-XLII-4-W18-923-2019)*  
76 *isprs-archives-XLII-4-W18-923-2019*
- 77 Shi F, Yang B, von Gunten L, Qin C, Wang Z (2011) Ensemble empirical mode decomposition  
78 for tree-ring climate reconstructions. *Theoretical and Applied Climatology* 109(12):233–  
79 243, DOI <https://doi.org/10.1007/s00704-011-0576-8>
- 80 Silva CB, Silva MES, Krusche N, Ambrizzi T, de Jesus Ferreira N, da Silva Dias PL (2018) The  
81 analysis of global surface temperature wavelets from 1884 to 2014. *Theoretical and*  
82 *Applied Climatology* 136(3-4):1435–1451, DOI [https://doi.org/10.1007/s00704-018-](https://doi.org/10.1007/s00704-018-2569-3)  
83 [2569-3](https://doi.org/10.1007/s00704-018-2569-3)
- 84 Torres ME, Colominas MA, Schlotthauer G, Flandrin P (2011) A complete ensemble  
85 empirical mode decomposition with adaptive noise. In: *2011 IEEE International*  
86 *Conference on Acoustics, Speech and Signal Processing (ICASSP)*, pp 4144–4147
- 87 Turner J, Colwell SR, Marshall GJ, Lachlan-Cope TA, Carleton AM, Jones PD, Lagun V, Reid  
88 PA, lagovkina S (2005) Antarctic climate change during the last 50 years. *International*  
89 *Journal of Climatology* 25(3):279–294, DOI <https://doi.org/10.1002/joc.1130>
- 90 Wang H, Mehta VM (2008) Decadal variability of the Indo-Pacific warm pool and its  
91 association with atmospheric and oceanic variability in the NCEP-NCAR and SODA

- 92 reanalyses. *Journal of Climate* 21(21):5545–5565, DOI  
93 <https://doi.org/10.1175/2008jcli2049.1>
- 94 Wu Z, Huang N (2009) Ensemble empirical mode decomposition: a noise-assisted data  
95 analysis method. *Advances in Adaptive Data Analysis* 1:1–41, DOI  
96 <https://doi.org/10.1142/S1793536909000047>
- 97 Wu Z, Huang NE, Wallace JM, Smoliak BV, Chen X (2011) On the time-varying trend in  
98 global-mean surface temperature. *Climate Dynamics* 37(3-4):759–773, DOI <https://doi.org/10.1007/s00382-011-1128-8>
- 100 Xing P, Chen X, Luo Y, Nie S, Zhao Z, Huang J, Wang S (2016) The extratropical northern  
101 hemisphere temperature reconstruction during the last millennium based on a novel  
102 method. *PLOS ONE* 11(1):e0146776, DOI  
103 <https://doi.org/10.1371/journal.pone.0146776>
- 104 Yang C, Wu H, Hu D (2011) Relationship between air temperature oscillations and solar  
105 variability on short and medium time scales. *Science China Earth Sciences* 54(6):912–  
106 923, DOI <https://doi.org/10.1007/s11430-010-4161-2>
- 107 Yang P, Wang G, Zhang F, Zhou X (2015) Causality of global warming seen from  
108 observations: a scale analysis of driving force of the surface air temperature time series  
109 in the northern hemisphere. *Climate Dynamics* 46(9-10):3197–3204, DOI <https://doi.org/10.1007/s00382-015-2761-4>
- 111 Zhou J, Tung KK (2013) Deducing multidecadal anthropogenic global warming trends using  
112 multiple regression analysis. *Journal of the Atmospheric Sciences* 70(1):3–8, DOI <https://doi.org/10.1175/jas-d-12-0208.1>
- 114 Ziliak ST, McCloskey DN (2004) The standard error of regressions in the *american*  
115 *economic review*. *Journal of Socio-Economics* 33(5):527–546, DOI  
116 <https://doi.org/10.1016/j.socec.2004.09.024>

## Supplementary Files

This is a list of supplementary files associated with this preprint. Click to download.

- [5 IMFdemod.r](#)
- [calcIMF8skewness.r](#)
- [calcenergies.r](#)
- [calctrendchanges.r extract](#)
- [nalimfstemp.r extract](#)
- [nalspectratemps.r iceemdan.r](#)
- [iceemdanP.r mhs.r](#)
- [printgraphs.r](#)
- [processtemperature.r](#)
- [processtemperaturenh.r](#)
- [processtemperaturesh.r](#)
- [processtemperaturetropics.r](#)
- 
- 
-